Turbid-Polyurethane Phantom for Microscopy

A. L. Dayton and S. A. Prahl

BME Dept., Oregon Health & Science University, Portland, OR

ABSTRACT

Calibration standards are needed for measurements of tissues in reflectance mode confocal microscopy. We have created a three dimensional turbid polyurethane phantom with a grid of inclusions. The grid had a 10 fold increase in absorption compared to the bulk of the phantom and the same scattering properties. India ink was used as an absorber for the bulk of the phantom, and Epolin 5532 (absorption peak at 500 nm) was used in the grid. Titanium dioxide particles were used as scatterers. The optical properties of the constructed phantoms were characterized with diffuse reflectance and transmission measurements followed by an inverse adding doubling method. At 488 nm the total attenuation coefficient was $40.6 \pm 0.3\,\mathrm{cm}^{-1}$ in the grid and $32.5 \pm 0.3\,\mathrm{cm}^{-1}$ in the bulk of the phantom. The phantom was imaged with reflectance mode confocal microscopy. Image analysis using the Beer-Lambert-Bouguer Law was performed. In the low absorbing bulk of the phantom the total attenuation coefficient was estimated accurately, however in the high absorbing grid, the total attenuation coefficient was underestimated by image analysis techniques.

keywords: Polyurethane, Phantom, Reflectance Mode Confocal Microscopy

1. INTRODUCTION

Polyurethane phantoms have many advantages as calibration standards. Pogue and Patterson's review[1] of optical phantoms compared the various materials commonly used for optical phantoms. Polyurethane is advantageous for several reasons: it is solid, permanent, machinable, and durable. When compared to epoxy resins, polyurethane has similar characteristics but has a shorter pot life of 30 minutes. It has also been shown that anthraquinone dyes are stable for at least a year in cured polyurethane.[2] Reflectance mode confocal microscopy has been used by many to image cells and tissues,[3,4,5,6] and some have measured the optical properties of tissue this way.[7] This paper explores some of the challenges of using reflectance mode confocal imaging to measure optical properties.

2. PHANTOM PREPARATION

The phantoms were created as described in Moffitt *et al.*[2] However, the phantom described in this work was inlaid with three dimensional absorption heterogeneities. Briefly, the first phase was to create the bulk of the phantom with known background optical properties. The second phase was to mill troughs into the background phantom. The third phase was to fill the voids with polyurethane having different optical properties.

2.1 Phase 1. Background Polyurethane

Polyurethane (BJB Enterprises, Inc.) was made from two components; component A was unreacted polyurethane and component B was catalyst, Figure 2. An absorber, india ink (PRO ART, Beaverton, OR), was mixed with component A and a scatterer, titanium dioxide, TiO_2, (Sigma, St. Louis MO) was mixed with component B. Each component was then placed in a vacuum chamber for degassing, the solutions were held at a reduced pressure until all air bubbles were drawn out of solution. The two components, A:B, were then mixed together in a 100:85 weight ratio respectively. After mixing, the uncured polyurethane was degassed again and then cast into a mold. To simulate a tissue with low background absorption, an absorption coefficient of about $1\,\mathrm{cm}^{-1}$ and a reduced scattering coefficient between 6 and $12\,\mathrm{cm}^{-1}$ was desired. India ink was added to component A at a concentration of $0.0025\frac{mL}{g}$ and a sonicated TiO_2 in ethanol stock ($4.93\frac{mg}{mL}$) was added to component B at a concentration of $0.014\frac{mL}{g}$. A phantom approximately 6 cm in diameter and 3 mm thick was cast; integrating sphere measurements were made on this phantom. In addition, a square phantom approximately, $6 \times 6 \times 1$ cm, this served as the bulk of the 3 dimensional phantom.

Further author information: (Send correspondence to S.A.P.)
S.A.P.: E-mail: prahl@bme.ogi.edu, Telephone: (503) 216-2197, 9205 SW Barnes Rd., Portland, OR 97225, USA

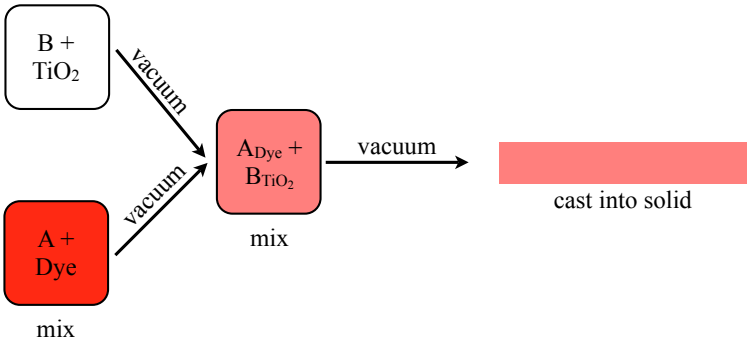

Figure 1: Simple illustration of the steps involved in making polyurethane phantoms.

2.2 Phase 2. Milling

After complete curing, 48 hours, the surface of the polyurethane phantom was milled flat (Sherline, San Marcos, CA) and the surface was then sanded smooth with 320 grit sand paper followed by 900 μm grit. A grid of troughs 1000, 700, 450 and 100 μm wide and 2 mm deep was then milled into the phantom.

2.3 Phase 3. Polyurethane Heterogeneity

The troughs were filled with polyurethane, Figure 2. While absorbance increased by a factor of 10 at 500 nm, scattering was kept the same as the bulk of the phantom. Epolin 5532 (Epolin Inc., Newark, NJ) absorbing dye and TiO_2 were used as absorbers and scatterers in the troughs of the phantom. TiO_2 was added to component B at the same concentration that was previously used in the bulk of the phantom $0.014\frac{mL}{g}$. A stock of Epolin 5532 dissolved in xylene (Fisher)$5.04\frac{mg}{mL}$) was added to component A at a concentration of $0.044\frac{mL}{g}$. As above, the two components were mixed together and degassed in a vacuum chamber. After degassing, a $3\,mL$ syringe was used to place the uncured polyurethane into the troughs of the milled phantom. The phantom was degassed a second time and then allowed to cure for 48 hours. After curing, the phantom was milled and sanded smooth.

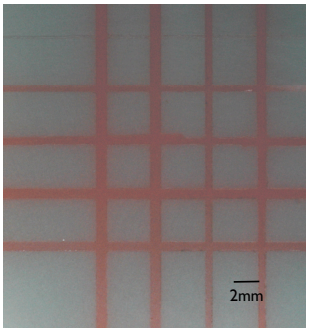

Figure 2: Polyurethane phantom, a low absorbing background inlaid with a grid of higher absorbing troughs at 500 nm.

3. PHANTOM CHARACTERIZATION

3.1 Total Diffuse Reflectance and Transmittance

To determine the optical properties of the cured polyurethane, integrating sphere measurements were made and inverse adding-doubling (IAD) was used.[2] A Xenon light was coupled to a 1 mm diameter fiber and used to make both reflectance and transmittance measurements with an integrating sphere (20.32 cm diameter sphere, 4.45 cm diameter sample port, 0.64 cm entrance port, 0.5 cm diameter illumination beam). The detector on the integrating sphere was a 1 mm diameter fiber that fed into a spectrometer (ISA Horiba) and then a PMT (Products for Research, Inc.) detector. The intensity of the light reaching the detector was measured, M. Both

dark noise, M_{dark} and 100%, M_{100} signals were measured for reflectance and transmission as well. A certified reflectance standard (Labsphere) was used for the 100% reflectance measurements. The signal, M was normalized as follows corresponding to either reflectance, R, or transmission, T.

$$R = \frac{M - M_{dark}}{M_{100} - M_{dark}} \tag{1}$$

$$T = \frac{M^{'} - M^{'}_{dark}}{M^{'}_{100} - M^{'}_{dark}} \tag{2}$$

Two 6 cm diameter and 3 mm thick scattering phantoms, one with India ink and one with Epolin 5532 as absorbers, were measured with the integrating sphere. Three reflectance and three transmission measurements were taken for each sample. An inverse adding-doubling method was used to calculate the absorption coefficient, μ_a, and the reduced scattering coefficient $\mu_{s'}$ from the normalized R and T measurements. The anisotropy of the phantoms was 0.8 and the scattering coefficientμ_s was calculated by

$$\mu_s = \frac{\mu_{s'}}{(1 - 0.8)} \tag{3}$$

and the total attenuation coefficient, μ_t, was calculated by

$$\mu_t = \mu_a + \mu_s \tag{4}$$

3.2 Confocal microscopy

3.2.1 Imaging

A Zeiss LSM 510 Meta Confocal Microscope was used to image the grid phantom. A 10×/0.5 objective was used. The angular aperture was 30°, lateral resolution 0.4 μm, axial resolution 4 μm, laser power 30 mW, and a pixel acquisition of 3.2 μs. An argon laser was used to excite the phantom at 458, 477, 488, and 514 nm. Collection filters were set to acquire light between 457 - 468, 468 - 479, 479 - 490, and 511- 522 nm and fluorescence of the Epolin 5532 dye between 533 - 618 nm, Figure 3. Reflectance and fluorescence signals were simultaneously collected through one pinhole, 39 μm in diameter. The inverted microscope images the phantom through a coverslip. Oil (Immersol 518 F, Zeiss, Germany) was placed between the coverslip and phantom to reduce the specular reflectance at the interface of the phantom (refractive index = 1.46). A three dimensional image was taken at the interface of a trough and background (900 × 900 × 700 μm, X×Y×Z), Figure 3. It should be noted that z=0 is not at the surface of the phantom, but rather 30μm past the surface.

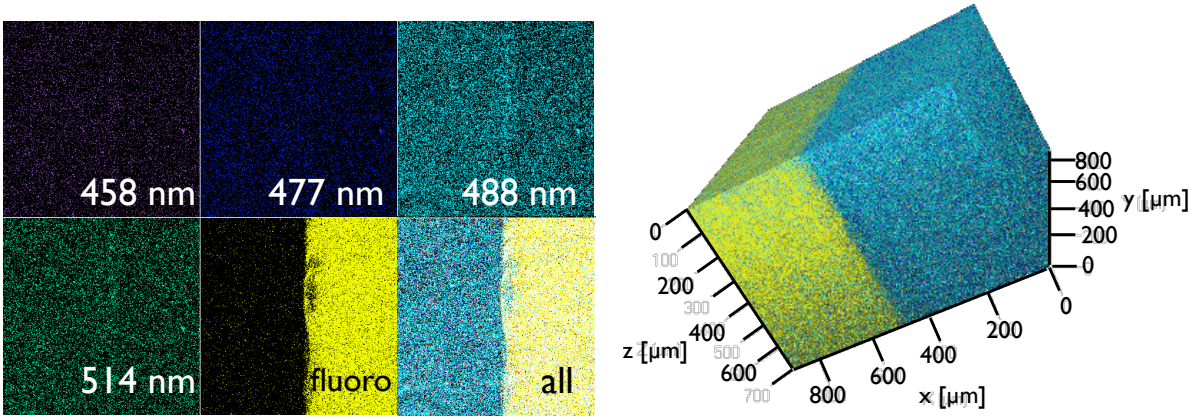

Figure 3: Left: Each of the five collection channels and the superposition of all the channels in one XY plane. Right: A three dimensional image of the interface between high absorbance trough and low absorbance background.

3.2.2 Image analysis

For each of the four excitation wavelength cubes the pixel intensity values were normalized to the maximum intensity.

$$I_n = I_i / I_{max} \tag{5}$$

Where I_n was the normalized intensity, I_i was the measured intensity, and I_{max} was the maximum intensity in the cube. Two regions of interest were selected within the 3D image, each was $161 \times 505 \times 337\,\mu$m, X×Y×Z, one in the high absorbing trough and the other in the low absorbing background.

The image was analyzed using two methods. First, a statistical approach was examined. The Beer-Lambert-Bouguer Law was expected to govern the decay of the reflectance confocal signal, I_n, in the axial direction.

$$I_n = e^{-2\mu_t z} \tag{6}$$

Equation 6 rearranged to solve for μ_t becomes

$$\mu_t = \frac{-\ln(I_n)}{2z} \tag{7}$$

where μ_t is the total attenuation coefficient, I_n is the normalized intensity of the pixel, z is the axial depth, and 2 accounts for the path length of light entering and leaving the phantom. An axial line is defined as the intensity through Z at each pixel (X_i, Y_j), Figure 4 shows the distribution of intensity values for one axial line. 150 axial lines from each region of interest were selected for analysis. Each pixel of each axial line was fit to equation 1. The median μ_t values of each axial line were normally distributed, Figure 4, therefore the mean of that distribution was used to represent μ_t.

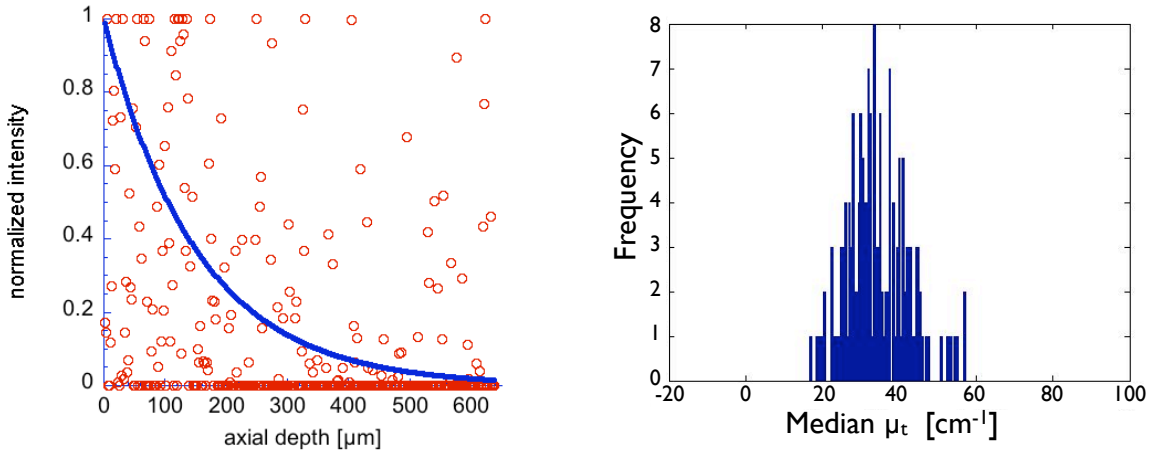

Figure 4: Left: Circles represent the intensity distribution of a single axial line. The line is equation 7 with μ_t equal to the mean μ_t from the graph on the right. Right: The median μ_t from 150 axial lines within the cube were normally distributed.

The second analysis method assumed that singly scattered photons were the brightest pixels in the image, or the maximum intensity pixels. The maximum normalized intensity values of 1 were counted for each XY plane. The sum of the maximum values in each XY plane fell off exponentially and μ_t was calculated by the Beer-Lambert-Bouguer Law as above.

$$C = a + be^{-2\mu_t z} \tag{8}$$

Where C is the number of maximum intensity values per axial depth, Figure 5, a and b are fitting parameters, μ_t is the total attenuation coefficient.

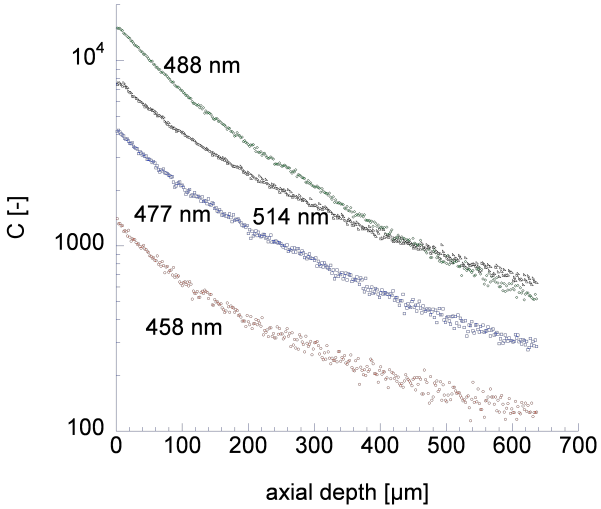

Figure 5: The number of maximum intensity values per XY plane for the background polyurethane.

4. RESULTS

4.1 Total Diffuse Reflectance and Transmittance

Figure 6 shows the optical coefficients for the background and trough portions of the phantom as calculated with integrating sphere measurements and IAD. For the india ink sample, μ_a is relatively constant at $1\,\mathrm{cm}^{-1}$. For the Epolin 5532 sample, a strong absorbance peak at 500 nm is observed. For both samples, $\mu_{s'}$ is approximately $6\,\mathrm{cm}^{-1}$ between 450 and 520 nm. Therefore, μ_s is approximately $30\,\mathrm{cm}^{-1}$ over the same range. Table 1 summarizes the calculated total attenuation coefficients.

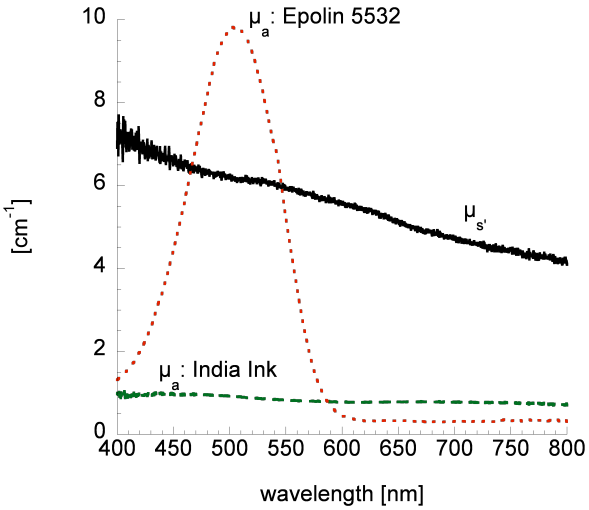

Figure 6: Optical coefficients for the polyurethane phantoms measured by diffuse reflectance and transmittance.

wavelength [nm]	μ_t [cm^{-1}]
background	
458	33.8 (0.6)
477	32.7 (0.4)
488	32.5 (0.3)
514	31.8 (0.3)
trough	
458	38.2 (0.6)
477	39.5 (0.4)
488	40.6 (0.3)
514	40.4 (0.3)

Table 1: Total attenuation, μ_t, of the background and trough portions of the 3D phantom as measured by diffuse reflectance and transmittance. Data reported as mean (standard deviation).

4.2 Confocal Microscopy

The calculated values for μ_t from reflectance mode confocal microscopy matched the values calculated from integrating sphere measurements for the low absorbing background, Figure 7. However, the confocal values are significantly lower than the expected values in the highly absorbing trough, Figure 7.

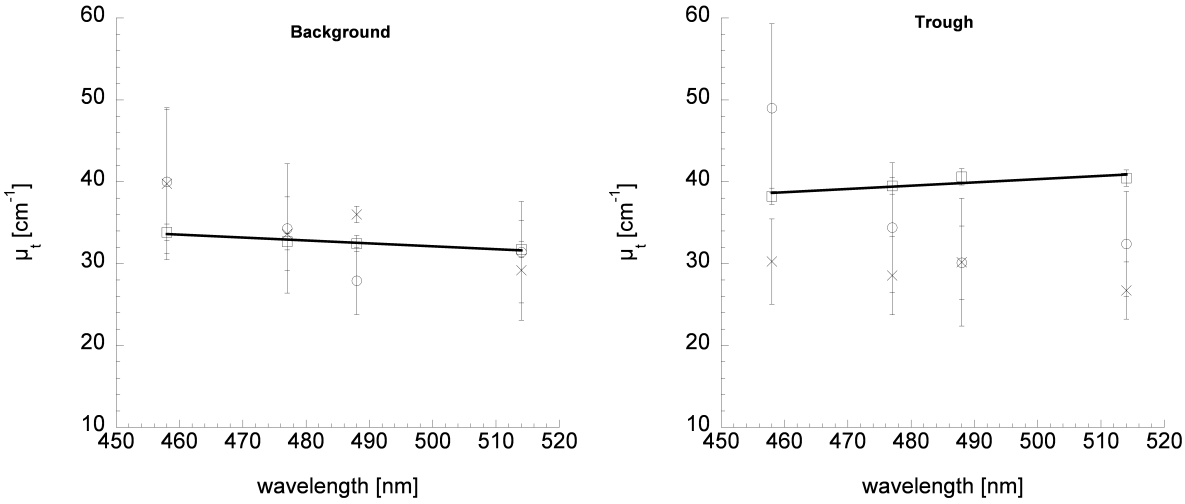

Figure 7: Values for μ_t calculated from IAD, squares; reflectance mode confocal microscopy statistical analysis, circles, and single scatter analysis, $\times$. Left: the low absorbing background and right: the high absorbing trough. Error bars are standard deviations and the line is fit through the IAD values.

5. DISCUSSION

Turbid polyurethane phantoms were constructed. The phantoms were measured with diffuse reflectance and transmission measurements and inverse adding doubling was used to determine their optical properties. For confocal microscopy, a phantom with a grid of inclusions with relatively higher absorption than the surrounding polyurethane was made and imaged three dimensionally. The Beer-Lambert-Bouguer Law was expected to govern the decay of the reflected confocal signal, as in equations 6 and 8. In the case of the low absorbing India ink, both image analysis methods approximated the total attenuation coefficient measured with diffuse reflectance and transmission. However, with the highly absorbing Epolin 5532 neither image analysis technique was able to approximate the expected total attenuation values. It is clear that an axial line cannot be approximated accurately with the Beer-Labert-Bouguer Law.

REFERENCES

1. B. W. Pogue and M. S. Patterson, "Review of tissue simulating phantoms for optical spectroscopy, imaging and dosimetry," *Journal of Biomedical Optics* **11**(4), p. 041102, 2006.
2. T. Moffitt, Y.-C. Chen, and S. A. Prahl, "Preparation and characterization of polyurethane optical phantoms," *Journal of Biomedical Optics* **11**(4), p. 041103, 2006.
3. D. S. Gareau, G. Merlino, C. Corless, M. Kulesz-Martin, and S. L. Jacques, "Noninvasive imaging of melanoma with reflectance mode confocal scanning laser microscopy in a murine model," *Journal of Investigative Dermatolog* **127**, pp. 2184–2190, 2007.
4. L. E. Meyer, N. Otberg, W. Sterry, and J. Lademann, "In vivo confocal scanning laser microscopy: comparison of the reflectance and fluorescence mode by imaging human skin," *Journal of Biomedical Optics* **11**, p. 04012, July/August 2006.
5. Y. Li, S. Gonzalez, T. H. Terwey, J. Wolchok, Y. Li, I. Aranda, R. Toledo-Crow, and A. C. Halper, "Dual mode reflectance and fluorescence confocal laser scanning microscopy for in vivo imaging melanoma progression in murine skin," *J Invest Dermatol* **125**, pp. 798 – 804, 2005.
6. C. Smithpeter, A. Dunn, R. Drezek, T. Collier, and R. Richards-Kortum, "Near real time confocal microscopy of cultured amelanotic cells: Sources of signal, contrast agents and limts of contrast," *Journal of Biomedical Optics* **3**, pp. 429–436, October 1998.
7. D. S. Gareau, *In vivo confocal microscopy in turbid media.* PhD thesis, Oregon Health and Science University, 2006.